CHEMISTRY OF MATERIALS

Article

pubs.acs.org/cm

Effect of Al_2O_3 Coating on Stabilizing $LiNi_{0.4}Mn_{0.4}Co_{0.2}O_2$ Cathodes

Anna M. Wise,[†] Chunmei Ban,[*,‡] Johanna Nelson Weker,[†] Sumohan Misra,[†,§] Andrew S. Cavanagh,[⊥] Zhuangchun Wu,[‡,#] Zheng Li,[○,∥] M. Stanley Whittingham,[○] Kang Xu,[△] Steven M. George,[⊥] and Michael F. Toney[*,†]

[†]Stanford Synchrotron Radiation Lightsource, SLAC National Accelerator Laboratory, 2575 Sand Hill Road, Menlo Park, California 94025, United States

[‡]Center of Chemicals and Materials Science, National Renewable Energy Lab, Golden, Colorado 80401, United States

[⊥]Department of Chemistry and Biochemistry, University of Colorado, Boulder, Colorado, United States

[○]Chemistry and Materials Science & Engineering, Binghamton University, Binghamton, New York, United States

[△]Sensor and Electronics Directorate, U.S. Army Research Lab, Adelphi, Maryland, United States

Supporting Information

ABSTRACT: Using atomic layer deposition of Al_2O_3 coating, improved high-voltage cycling stability has been demonstrated for the layered nickel−manganese−cobalt pseudoternary oxide, $LiNi_{0.4}Mn_{0.4}Co_{0.2}O_2$. To understand the effect of the Al_2O_3 coating, we have utilized electrochemical impedance spectroscopy, operando synchrotron-based X-ray diffraction, and operando X-ray absorption near edge fine structure spectroscopy to characterize the structure and chemistry evolution of the $LiNi_{0.4}Mn_{0.4}Co_{0.2}O_2$ cathode during cycling. Using this combination of techniques, we show that the Al_2O_3 coating successfully mitigates the strong side reactions of the active material with the electrolyte at higher voltages (>4.4 V), without restricting the uptake and release of Li ions. The impact of the Al_2O_3 coating is also revealed at beginning of lithium deintercalation, with an observed delay in the evolution of oxidation and coordination environment for the Co and Mn ions in the coated electrode due to protection of the surface. This protection prevents the competing side reactions of the electrolyte with the highly active Ni oxide sites, promoting charge compensation via the oxidation of Ni and enabling high-voltage cycling stability.

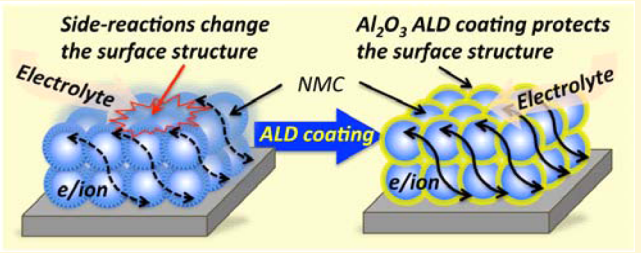

INTRODUCTION

The design of safe, high capacity electrochemical energy storage systems, herein lithium-ion batteries, with long cycle lifetimes requires a fundamental understanding of the chemical and physical processes that occur at the complex interface of electrodes with electrolytes. This understanding can then be applied to ultimately stabilize the electrochemical properties of these devices through surface and interface engineering.[1−4] Surface coating has been recently explored as one of most efficient strategies to functionalize or stabilize the surface, thereby modifying the interphase phenomena toward better facilitating charge transfer during lithium insertion/extraction.[5−7] Based on sequential self-limiting surface reactions, atomic layer deposition (ALD) has proven to be the best method to deposit continuous, conformal, and pinhole free films at low-temperature.[8] In previous work, we have demonstrated that Al_2O_3 ALD coatings (≤1 nm thick) greatly improve cycling stability of electrodes including widely used $LiCoO_2$.[9,10]

The demand of low-cost, safe, and less-toxic cathode materials has motivated the exploration of low-cobalt content layered oxides with a general formula of $LiNi_yMn_yCo_{(1-2y)}O_2$ ($0 < y \leq 1$).[11−15] Higher storage capacity and better thermal stability have been observed with the increasing substitution level of Ni and Mn,[16,17] but high substitution level of Ni and Mn results in low rate capability and dissolution of transition metals. Surface modification again shows its capability to improve the cycling stability.[18−22]

Recently, to understand the mechanism underlying the improved electrochemical performance, in situ X-ray diffraction (XRD), X-ray photoelectron spectroscopy (XPS) and transmission electron microscopy (TEM) have been used to study the structure of $LiCoO_2$.[23−28] However, little research has been devoted to how the surface modification affects the structural and surface chemistry evolution for $LiNi_yMn_yCo_{(1-2y)}O_2$ ($0 < y \leq 1$) electrodes. Despite having a similar layered structure to $LiCoO_2$, the mixed transition metal oxides ($LiNi_yMn_yCo_{(1-2y)}O_2$ ($0 < y \leq 1$)) have the transition metal involvement in the electrochemical reactions. The Ni and Mn substituted oxides have significantly more complicated surface

Received: July 30, 2015
Revised: August 21, 2015
Published: August 24, 2015

DOI: 10.1021/acs.chemmater.5b02952
Chem. Mater. 2015, 27, 6146−6154

chemistry and also show different structural changes during lithium extraction.[29] This can result in a different electrochemical behavior, such as a one-phase intercalation process instead of the two-phase process in the $LiCoO_2$, at ~3.9 V.[29] Therefore, with the aim of understanding the changes in mechanism as a result of surface coating the mixed transition metal oxides, we selected a highly substituted compound, $LiNi_{0.4}Mn_{0.4}Co_{0.2}O_2$, and utilized the binder-free technique developed in our lab to exclude the influence from any possible coating by the polymer binder additive, as well as mitigate the low conductivity in the highly substituted oxide electrode.[30,31] Single-walled carbon nanotubes have been used to fabricate the flexible conductive matrix accommodating the active material, $LiNi_{0.4}Mn_{0.4}Co_{0.2}O_2$, without adding any polymer binder additive. Operando XRD, operando X-ray absorption near-edge structure (XANES) spectroscopy, and in situ electrochemical impedance spectroscopy (EIS) were performed to systematically investigate how the coating affects the evolution of the structure and chemistry during lithium extraction and insertion.

Here we show that the Al_2O_3 coating prevents severe reactions with the electrolyte that are seen in the bare electrodes above 4.4 V, but does not restrict lithium intercalation or deintercalation. Our measurements reveal that the Al_2O_3 coating has an impact at lower voltages (<4.4 V), as evidenced by a delay in the involvement of Co and Mn ions in delithiation reactions at the start of lithium deintercalation. This delay is attributed to the protection of the surface chemistry, in particular the highly active Ni oxide sites, which promotes charge compensation via oxidation of Ni by preventing the competing side reactions of the electrolyte and enables the observed high voltage, high rate cycling stability.

EXPERIMENTAL SECTION

Material Synthesis and Cell Construction. The $LiNi_{0.4}Mn_{0.4}Co_{0.2}O_2$ (NMC) sample was synthesized by high-temperature solid-state heating. The detailed synthesis has been published elsewhere.[14] SWNTs produced by the laser vaporization method were purified by an HNO_3 reflux/air oxidation procedure.[32]

The binder-free electrode composed of $LiNi_{0.4}Mn_{0.4}Co_{0.2}O_2$ (95 wt %, with a particle size of about 80 nm)[31] and SWNTs (5 wt %) (referred to hereafter as NMC−CNT) was made by using $LiNi_{0.4}Mn_{0.4}Co_{0.2}O_2$−SWNTs suspension in deionized water with 1% concentration of sodium dodecyl sulfate as the surfactant. The NMC−CNT electrode was then fabricated by vacuum filtration, as reported by our previous work.[30,31] The NMC−CNT electrode was then baked in air at 300 °C prior to electrochemical testing.

Al_2O_3 ALD coating was grown directly on the $LiNi_{0.4}Mn_{0.4}Co_{0.2}O_2$ particles at 120 °C. For the Al_2O_3 ALD, TMA (97%) and HPLC (high performance liquid chromatography) grade H_2O was obtained from Sigma-Aldrich without further treatments. The typical growth rate for the chemistry is 1.1−1.5 Å per ALD cycle. Four ALD cycles were used to coat the NMC−CNT particles for ~6 Å thickness of coating. The detailed ALD reaction sequences were described in a previous report.[10] The Al_2O_3 coated electrodes were prepared in the same manner as the NMC−CNT electrodes and are referred to subsequently as ALDNMC−CNT.

The NMC−CNT electrode was used as a working electrode without adding any polymer binder additives. Aluminum foil (20 μm thick) was used as the current collector. Lithium metal (0.75 mm thick) was used as the counter electrode. The NMC−CNT electrodes were prepared with thicknesses of about 20 μm and similar loadings of active material (90−95%, average mass loading of 2−3 mg cm^{-2}). 2032 coin cells were used to characterize the electrochemical properties. For the operando X-ray measurements, two collinear 5 mm diameter windows were machined into the commercially available 2032 cells. These windows were sealed by affixing Kapton film (7 μm) to both the inside and the outside of each of the outer cell casings using epoxy (Loctite). All of the cells were assembled in an argon-filled drybox with oxygen and water levels of less than 0.5 ppm. A Celgard separator 2325 and 1 M $LiPF_6$ electrolyte solution in 1:1 w/w ethylene carbonate: diethyl carbonate ($LiPF_6$ in 1:1 EC/DEC, purchased from Novolyte) were used to complete the coin cells.

1% Tris(hexafluoro-iso-propyl) phosphate (HFiP) was used as an electrolyte additive in order to further improve the high-voltage electrochemical performance. To isolate the impact of the Al_2O_3 coating, HFiP was not added to the electrodes characterized by EIS, XRD, or XANES.

Electrochemical Characterization. Computer-controlled VMP3 channels (Bio-Logic Science Instruments SAS) were used to carry out electrochemical measurements. All of the cells were cycled at 0.1C (17 mA g^{-1}) for the first 10 cycles before cycling at higher rates.

The AC impedance was performed through a computer controlled Bio-Logic VMP3 analyzer. All of the EIS data were collected at designed charged/discharged states with a 5 mV AC signal ranging from 100 kHz to 10 mHz. In addition to using a very slow charging/discharge rate (0.02C), a 10 h rest is also applied before any EIS tests to equilibrate the interfacial and bulk reactions.

Operando X-ray Diffraction. XRD measurements were recorded during the charge and discharge of NMC−CNT and ALDNMC−CNT electrodes using a 2D Mar345 image plate detector (Rayonix) at beamline 11−3 at Stanford Synchrotron Radiation Lightsource (SSRL), SLAC National Accelerator Laboratory, with an X-ray energy of 12.74 keV. The measurements were recorded in transmission geometry with a beam size of 50 μm × 50 μm, a detector pixel size of 150 μm × 150 μm, and a sample-to-detector distance of 145 mm. The cells were cycled using a current density of 40 mA g^{-1}, charging to 4.7 V and discharging to 2.5 V vs Li/Li^+. XRD data were collected at 3.5 min intervals with an exposure time of 120 s. Data were calibrated using the peaks from the aluminum current collector as an internal reference, with the data reduction carried out using Area Diffraction Machine.[33] Data are plotted as a function of the scattering vector Q, where $Q = (4\pi\sin\theta)/\lambda$, where λ is the X-ray wavelength and θ is the Bragg angle.

Operando X-ray Absorption Spectroscopy. Operando XAS measurements were performed in transmission geometry at the Mn, Co and Ni K edges at beamline 4−1, SSRL. Beamline 4−1 is equipped with a Si(220) double-crystal monochromator and harmonic rejection was achieved by detuning the monochromator by 40−50%. Spectra were collected during a charge/discharge cycle for fresh coated and bare electrode cells at each absorption edge (six cells). XAS data were collected at OCV for each cell prior to starting the charge/discharge cycle at a rate of $C/8$ then collected continuously over the charge/discharge cycle (collection time for a single spectrum was approximately 20 min). The cells were charged to 4.5 V, held at 4.5 V for 30 min, and then discharged to 2.5 V vs Li/Li^+.

The data were processed and analyzed using ATHENA, part of the IFEFFIT software suite.[34] Incident X-ray energy calibration was carried out using the spectrum of the appropriate Mn, Co or Ni reference foil recorded simultaneously with the sample data. All spectra were calibrated, normalized, and background-subtracted. Quantitative assessment of each spectrum to determine the relative conversion to $x = 0.5$, where $Li_{(1-x)}Ni_{0.4}Mn_{0.4}Co_{0.2}O_2$, was carried out by linear combination fitting (LCF). The spectra recorded at OCV and at $x = 0.5$ of the bare samples were used as the reference spectra for both the bare and coated samples at each edge.

RESULTS AND DISCUSSION

Electrochemical Performance. The NMC−CNT binder-free electrodes comprised only $LiNi_{0.4}Mn_{0.4}Co_{0.2}O_2$ and SWNTs have been reported to have great rate-performance with an operating voltage range from 3.0 to 4.2 V.[31] Although the Ni and Mn highly substituted structure has lower electronic conductivity than $LiCoO_2$,[16] the SWNTs-enabled matrix

DOI: 10.1021/acs.chemmater.5b02952
Chem. Mater. 2015, 27, 6146−6154

ensures great electronic wiring in the composite electrode. Therefore, the binder-free SWNTs-enabled electrodes have significantly improved electrochemical kinetics, much higher capacity retention at high cycling rates, and lower impedance compared to electrodes without the chemically bound SWNT matrices.[30,31] Following this research, we compare the rate performance between NMC−CNT electrodes and Al_2O_3 ALD coated electrodes (denoted as ALDNMC−CNT).

Figure 1 compares the cycling performance of the bare NMC−CNT and 6 Å ALD Al_2O_3 coated NMC−CNT

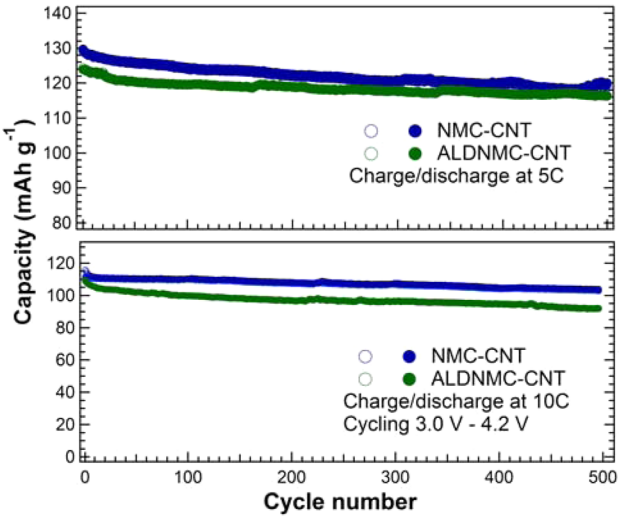

Figure 1. High-rate capability of both the bare and ALD Al_2O_3 coated NMC−CNT electrodes at 5*C* (top) and 10*C* (bottom) over 500 cycles, cycled between 3.0−4.2 V vs Li/Li$^+$. Hollow symbols represent the charging capacity, whereas solid symbols represent the discharging capacity.

electrodes at high cycling rates of 5*C* and 10*C* (full capacity reached following 12 and 6 min, respectively) within a voltage window of 3.0−4.2 V. Remarkable highly stable cycling performance is seen for both electrodes which is in agreement with our previous results,[30,31] and is attributed to the highly conductive CNT matrix chemically bound to the surface of the NMC. The NMC−CNT exhibits an initial discharge capacity of 130 mAh g^{-1} at 5*C* and high capacity retention (92%) after 500 cycles. In the Al_2O_3-coated NMC−CNT electrode (ALDNMC−CNT), the electronically insulating Al_2O_3 coating can delay the electron transfer so as to negatively affect the rate capability. With the ultrathin insulating coating (∼6 Å), the ALDNMC−CNT offers a slightly lower capacity of 125 mAhg^{-1} and similar capacity retention (93%) after 500 cycles. These results are consistent with our previous results in which the Al_2O_3 coated $LiCoO_2$ electrode shows lower capacity at higher cycling rate.[9] In our previous studies, it was also found that the electronic conductivity decreases as the coating thickness increases.[9] Therefore, a thin coating is preferred to maintain the high-rate capability.

Because of displaying better structural and thermal stability than $LiCoO_2$, $LiNi_{0.4}Mn_{0.4}Co_{0.2}O_2$ has the potential to be cycled at higher cutoff voltages than 4.3 V.[35] Figure 2 shows data on representative rate capability (discharge capacity vs cycle number at different *C* rates as indicated) of bare and coated electrodes, when cycling between 2.5 and 4.5 V. With a low cutoff voltage (Figure 1), the bare electrodes behave similarly to the coated electrodes in terms of stability, whereas

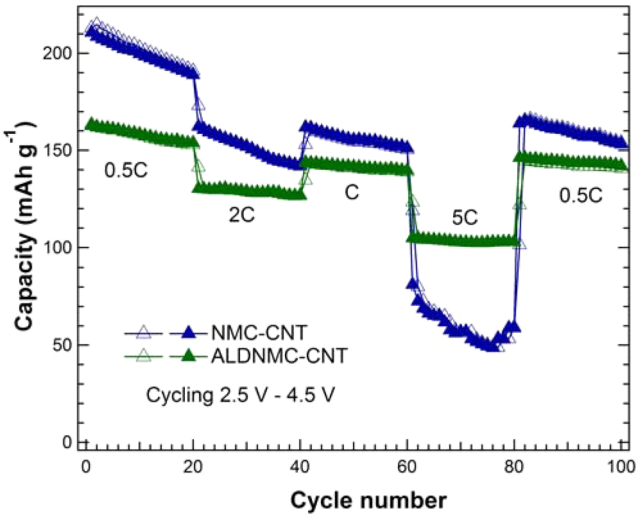

Figure 2. High-voltage cycling performance of the bare and Al_2O_3 ALD coated NMC−CNT electrodes cycled between 2.5 and 4.5 V vs Li/Li$^+$. Hollow symbols represent the charging capacity, whereas solid symbols represent the discharging capacity.

the coated electrodes demonstrate slightly lower capacities due to the coating's insulating property. In contrast, a fast decay in capacity was observed in the bare NMC−CNT electrode when cycling the electrodes with the higher cutoff voltage (4.5 V). Stable electrochemical performance in terms of rate capability and cyclability has been demonstrated at various cycling rates (e.g., 0.5−5*C*) on the coated electrodes. However, slightly lower capacities were achieved in ALDNMC−CNT electrodes than that in NMC−CNT. It is believed that the strong interaction between the surface of the cathode and the electrolyte causes additional irreversible capacity for bare $LiNi_{0.4}Mn_{0.4}Co_{0.2}O_2$.[3] The protective Al_2O_3 coating blocks the direct contact between surface of the cathode and the electrolyte, ultimately preventing the additional irreversible capacity. If the products from the irreversible reactions fail to passivate the surface, the parasitic reactions will continue to corrode the surface of cathode and result in fast degradation. Not surprisingly, capacity fading was observed in NMC−CNT electrodes at various cycling rates, and worsens at higher cycling rates.

Further enhancement in the rate performance at higher voltage has been achieved when using HFiP as an electrolyte additive. The HFiP has been proven to minimize impedance at the cathode surface.[5] As shown in Figure S1, the stable superior capacity of the Al_2O_3-coated electrode has confirmed the dual-protection by both the Al_2O_3 ALD and the HFiP additive in minimizing undesirable side reactions and/or dissolution of the positive electrode, leading to capacities of 180 mAh g^{-1} and 160 mAh g^{-1} at cycling rates of 2*C* and 5*C*, respectively. To better understand the coating's effect on the structural and chemical changes, we have use the typical carbonate electrolyte ($LiPF_6$ in 1:1 EC/DEC) to perform the in situ and operando analyses of NMC−CNT and ALDNMC−CNT electrodes without adding HFiP additive.

Electrochemical Impedance Spectroscopy. To understand the mechanism of the capacity fading at voltages above 4.2 V, we measured the electrochemical resistance of the bare and coated NMC−CNT cathodes using EIS. EIS measurements were performed at different states of charge/discharge, under the 0.02*C* rate (3.4 mA g^{-1}). During the first charge and

DOI: 10.1021/acs.chemmater.5b02952
Chem. Mater. 2015, 27, 6146−6154

discharge, 20 EIS measurements were collected at the potentials indicated in Figure 3. The Nyquist plots of these

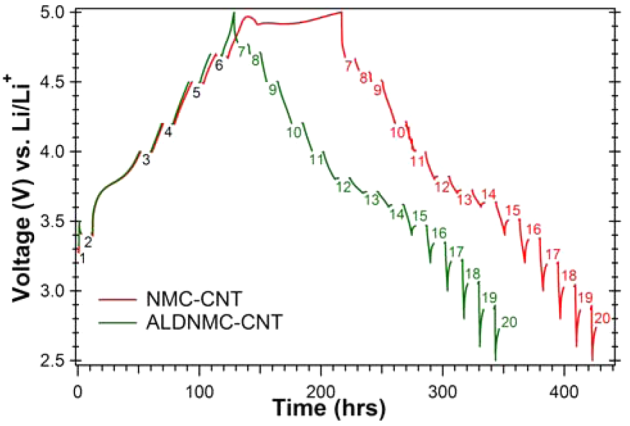

Figure 3. Quasi-open circuit voltage curve of the first charge and discharge of NMC−CNT and ALDNMC−CNT vs Li cells obtained by the galvanostatic intermittent technique (GITT). The cell was charged/discharged at a 3.4 mA g^{-1} rate (C/50) for the preset voltages (labeled by numbers) and then allowed to rest for 10 h before taking EIS.

EIS measurements depicting the imaginary part of the impedance versus the real part of the impedance, with high frequency data corresponding to low values of the real part, are plotted in Figure 4. The interpretation of the impedance signals is based on the equivalent circuit comprised of resistance (R), constant phase element (CPE, replacing the ideal capacitor) and Warburg term (W) related to the solid-state Li^+ diffusion into the bulk, shown in Figure 4.[3] The fitting curves, also plotted in Figure 4, indicate the obtained impedances can be fit well to the equivalent circuit. On the basis of the Voigt-type model, R_s is the resistance associated with the cell components including the electrolyte, separator and the electrodes. R_{int} is the interface resistance relevant to the SEI film, which is related to the high-frequency (HF) semicircle. R_{ct} is the charge-transfer resistance for the electrode reaction, which determines the midfrequency (MF) semicircle.

During the charging, the R_{int} in both bare and coated electrodes decreases initially, then increases at the end of charge. Recently, the HF semicircle has been interpreted as an interphase contact resistance in the electrode bulk.[36] During charging, the lithiated SWNTs enhance the contact between active materials and SWNTs, resulting in smaller HF semicircle at lower voltages. But the decomposition of the electrolyte and the interaction between the electrolyte and the surface of the layered oxide, present at higher voltages (>4.4 V), lead to the formation of insulating interfacial layers on the surface of the cathode.[3] Thus, a dramatic increase of R_{int} is observed in the uncoated NMC−CNT electrode. Note that the surface reaction between electrolyte and cathode contributes a large capacity gain between 4.7 and 5 V, as confirmed in Figure 3. It is known that highly delithiated layered oxides are not stable, but very reactive, which can trigger the interaction between the unstable electrolyte (above 4.4 V) and the surface of cathode.[5] In the case of $LiNi_{0.4}Mn_{0.4}Co_{0.2}O_2$, the nucleophilic oxygen bound to the high content of Ni can cause pronounced interaction between the layered oxides and the carbonate electrolyte.[37] This leads to massive surface film precipitation, which causes the slow solid-state diffusion through the "newly" formed layer.

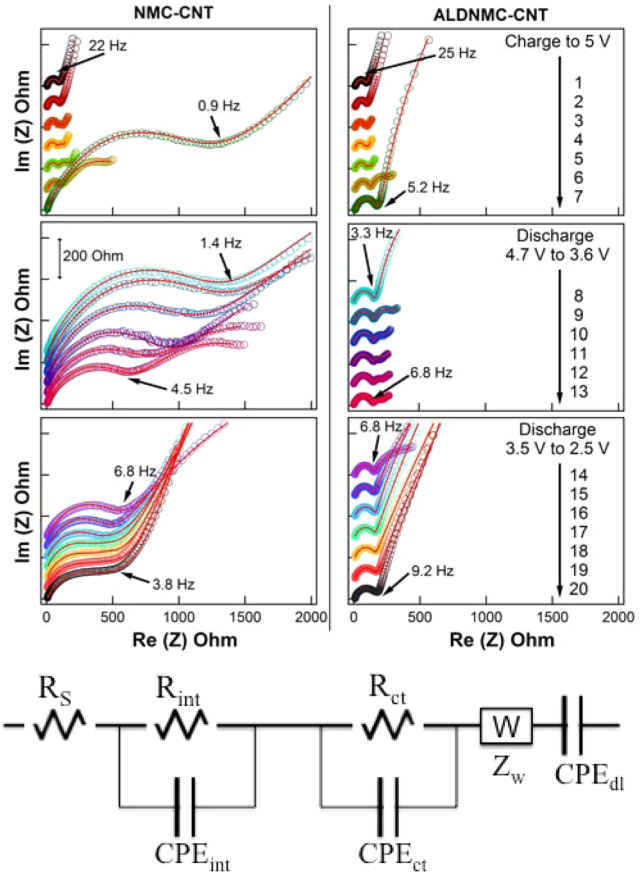

Figure 4. Nyquist plots (open circles) and fitting curves (red lines) from the NMC−CNT and ALDNMC−CNT half cells. Left and right columns display the plots from NMC−CNT and ALD-coated cathodes, respectively. The symbols represent the EIS measurement data, and the lines are fitting curves using the equivalent circuit. All of the axes have the same scale. The equivalent circuit used for the EIS fitting is shown below the Nyquist plots.

As a consequence, the bare NMC−CNT shows large impedance above 4.5 V even during the discharge. In addition, a MF circle can be seen in the EIS spectra of the bare NMC−CNT electrode recorded between 4.0 and 4.5 V, symptomatic of an increase in the charge transfer resistance prior to the large increase in R_{int}.

In contrast, the total impedance in the coated ALDNMC−CNT cathode only increases slightly, even when charged to 5 V. With the protective layer, the interaction between the electrolyte and the reactive cathode was largely mitigated. No obvious increase in R_{int} indicates that the Al_2O_3 coating is chemically stable against the reactive electrolyte, even when cycling at the high voltages (beyond the oxidation potential of the carbonate electrolyte). The results further confirm that uniform and conformal coverage has been achieved by using the ALD technique. Finally, it is because of the atomic level coating of the insulating material that the total impedance of the coated electrode is barely affected. Therefore, the seamless coating with a thickness about 6 Å prevents the direct contact between electrolyte and surface of the cathode, and significantly suppresses the decomposition of the electrolyte on the surface of cathodes. Thus, a stabilized surface with only slight changes in impedance was obtained in the coated electrode. Moreover, there is no extra capacity observed in the ALD-coated cathode.

DOI: 10.1021/acs.chemmater.5b02952
Chem. Mater. 2015, 27, 6146−6154

The impedance of the bare electrode starts decreasing during discharging, but the impedance at the end of discharge for the bare electrode is still much larger than the fresh electrode. The decreased impedance indicates the partial dissolution of the interfacial layer resulting in relatively low impedance.[10] However, the impedance data of the coated cathode show much smaller HF and MF semicircles than those in the bare electrode, and indicate a stable and clean surface for the coated electrode during the cycling.

Operando X-ray Diffraction. Synchrotron-based operando XRD was performed to investigate the structural evolution of the bare and coated cathodes during the first cycle. A total of 224 XRD scans were collected during the galvanostatic cycling with a potential limit of 4.7 V. This upper limit of 4.7 V was chosen rather than 5 V to avoid the significant increase in impedance seen above 4.7 V. Figures S2 and S3 show the voltage profiles of the NMC−CNT/Li and ALDNMC−CNT/Li cells as a function of time. Figure 5 shows representative XRD patterns with Bragg reflections from the (003) through the (102) peaks. The full diffraction patterns recorded are reported in Figures S4 and S5. The peak around 1.55 $Å^{-1}$ is attributed to crystallization of the well-bundled SWNTs. The peaks at around 2.55 $Å^{-1}$ and 3.69 $Å^{-1}$ belong to the lithium metal, used as the counter electrode. The peaks from the aluminum current collector were also observed at around 2.65 and 3.05 $Å^{-1}$. All other peaks can be indexed to a single phase with the layered α-$NaFeO_2$ structure.[13,30] The structure consists of a cubic close-packed arrangement of the oxide ions. The transition metal ions in the structure occupy alternating layers in the octahedral sites.

Figure 5 shows a smooth and gradual shift of the reflections, without the appearance of new peaks for both bare and coated cathodes. It indicates a single-phase, solid solution mechanism that preserves the stacking sequence. Close inspection of the (003) reflection (the Q space region between 1.2 and 1.5 $Å^{-1}$), which is directly related to the distance between transition metal layers, reveals an expansion of the c lattice parameter (shift to lower Q) during the charge, with a subsequent lattice contraction. At the end of charge at 4.7 V, the cells were held at a voltage of 4.7 V for 1 h. During the voltage hold, the (003) peak moves to even higher Q values, indicating a further decrease in the interlayer spacing. Inspection of the (101) peak (Q space region between 2.55−2.65 $Å^{-1}$) reveals a shift to higher Q, corresponding to a decrease in the d-spacing, during the charge with a subsequent shift to lower Q upon discharging. The (101) contains a major contribution from the a-axis (1/3 weight is from the c parameter),[38] and thus a contraction and expansion of the a lattice parameter can be inferred. These results are consistent with previous findings.[30,39] The strong peak at 2.55 $Å^{-1}$ from the crystalline structure of lithium metal shields the changes in the (101) peak and prevented further interpretation.

During the complete cycle there are no new peaks observed, and all of the shifts appear reversible when plotted as shown in Figure 5 and Figures S4 and S5. The reversible solid solution phase transition is in contrast with that of $LiCoO_2$ at the higher state of charge, where a two-phase transformation is observed.[29] The results further confirm the impact of Ni and Mn substituents on the structural transitions during lithium removal.[40]

To investigate the effect of ALD coating on the structural evolution of the NMC−CNT cathode, the change in the d-spacing for the (003) peak was plotted in Figure 6 as a function

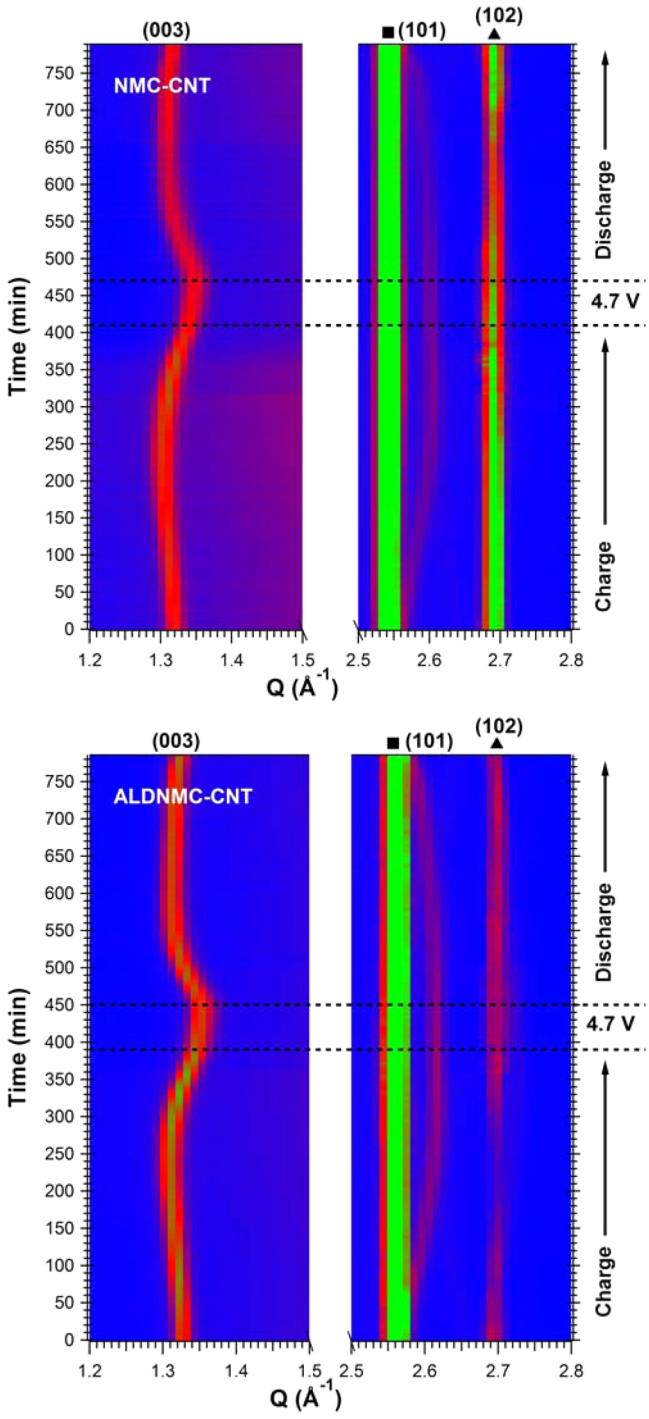

Figure 5. Operando XRD data of the bare (top) and Al_2O_3 ALD-coated (bottom) NMC−CNT electrodes within a selected Q space showing the (003), (101), and (102) peaks. XRD data were collected during the delithiation/lithiation cycle between 2.5−4.7 V vs Li/Li^+ using a current density of 40 mA g^{-1}. The two strong peaks at 2.55 $Å^{-1}$ (■) and 2.68 $Å^{-1}$ (▲) are from the lithium metal and the aluminum current collector, respectively. The peak (102) overlaps with the peak from the Al current collector.

of lithium content in the $Li_{(1-x)}Ni_{0.4}Mn_{0.4}Co_{0.2}O_2$ ($0 \le x \le 1$) cathodes (x was derived from the current using a theoretical capacity of 278.7 mAh g^{-1}, corresponding to complete Li extraction). The d-spacing can be seen to increase with charging, with a slight delay in the onset of the increase for the coated electrode compared to the bare. A maximum in the

DOI: 10.1021/acs.chemmater.5b02952
Chem. Mater. 2015, 27, 6146−6154

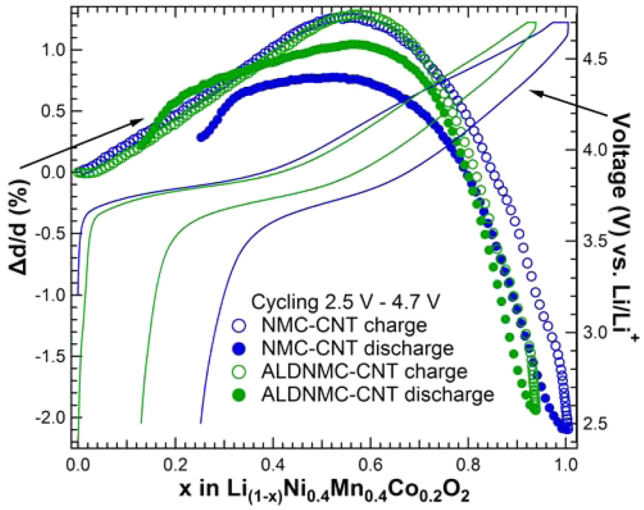

Figure 6. Percent shift (indicated by circles) in the (003) peak position as a function of x ($Li_{(1-x)}Ni_{0.4}Mn_{0.4}Co_{0.2}O_2$) determined from operando XRD data for both bare and coated NMC−CNT cathodes. Voltage profiles are also shown (indicated by lines) for each electrode as a function of x.

interlayer distance is reached at ∼ $Li_{0.5}$, followed by a contraction. The d-spacing continues to decrease during the voltage hold (at x = 0.92 for the coated electrode and x = 0.97 for the bare electrode), indicating a further change in structure. Both bare and coated NMC−CNT electrodes share a similar transition in d-spacing during the early stages of deintercalation up until 70% of the lithium is removed (∼4.3 V). Upon charging to voltages higher than 4.3 V, the capacity increase for the bare electrode is significantly greater than that for the coated electrode; however, the shift in the d-spacing is comparable. This suggests that a portion of the capacity gained above x = 0.7 is independent of changes to the crystal structure for the bare electrode. The extra capacity gain observed in the bare electrode is consistent with the conclusions from our EIS analysis described in an earlier section. Most likely, the capacity is attributed to the interaction between the electrolyte and the surface of the cathode, which also causes the precipitation of the interfacial layer.

During the discharge, the d-spacing for both bare and coated electrodes increases and then decreases after reaching x = 0.6. Although the shifts in d-spacing are not fully reversible for either electrode, the coated electrode shows a higher level of reversibility in terms of capacity and much higher Coulombic efficiency (CE, 86% in the coated electrode vs 76% in the bare electrode). Overall, the shifts in d-spacing are comparable for both the bare and coated electrodes. These results confirm that the coating does not constrain the structural evolution during the extraction and insertion of lithium ions, but does help to preserve the electrochemical behavior during cycling. It is worth noting that the operando XRD experiments used a much higher cutoff voltage (upper limit of 4.7 V, holding at 4.7 V for 1 h) than the normal charge limit (4.2 V). Cycling at high voltages caused the severe side reactions and decomposition of the electrolyte; resulting in the low CE, as well as high impedance during charge the transfer reactions.

Operando X-ray Absorption. XANES measurements were carried out to further investigate the effect of the Al_2O_3 coating, in particular at lower voltages. Both the EIS and XRD data show that the Al_2O_3 coating prevents the irreversible capacity caused by severe interaction of the electrode with the electrolyte at potentials above 4.4 V, but little variation between the bare and the coated electrodes below this voltage was detected. XANES is sensitive to both the oxidation state and coordination environment of an element, which are related to the energy of the X-ray absorption edge and the shape of the spectrum, respectively. The chemistry of the transition metal ions during cycling was therefore investigated by continuously recording XANES data over a charge/discharge cycle. An upper voltage cutoff of 4.5 V was used to avoid the severe side-reactions seen in the impedance and XRD data at higher voltages. Representative charge/discharge cycles for the NMC−CNT and ALDNMC−CNT electrodes recorded during the operando XANES measurements are shown in Figure S6.

Selected XANES spectra recorded at particular points (OCV of pristine cell, x = 0.5, charged to 4.5 V and discharged to 2.5 V) during the charge/discharge cycle of the bare and ALD coated cells at each absorption edge are shown in Figure 7a, c, e. The greatest change in oxidation state upon charging to 4.5 V is observed for the Ni (Figure 7a). This can be attributed to the oxidation of Ni from Ni^{2+} to Ni^{3+} then Ni^{4+} in accordance with previous studies.[41,42] Upon charging to a capacity where half of the Li has been removed (x = 0.5), it can be seen that Ni K edge XANES of both the coated and bare electrodes overlay, however, with further charging to the voltage limit of 4.5 V, no additional shift is seen in the bare electrode, whereas the ALD electrode shifts to a slightly higher oxidation state. Following discharge to 2.5 V, the Ni in the ALD electrode is reduced to its initial state, showing reversible cycling behavior; however, the Ni in the bare electrode does not completely return to the original state. It is also interesting to note that the XANES spectra recorded at OCV differ for the coated and bare electrodes, with the shoulder at ∼8347 eV more prominent in the bare electrode. This difference could be due to modification of the Ni environment at the surface as a result of contact with the electrolyte in the bare electrode or from an interaction with the Al_2O_3 layer in the coated electrode. For a surface effect to be apparent in this K edge XANES data, a bulk average measurement, there would need to be a reasonable proportion of the Ni at the surface of the particles, thus suggesting some preferential segregation of the Ni at the surface may be occurring as has been seen in studies of Li-, Mn-rich NMC.[43]

The Co and Mn XANES spectra (Figure 7c, e) recorded at OCV reveal no differences in the fresh electrodes as a result of ALD coating. A shift in the XANES is seen at both edges following charging to 4.5 V. In the case of the Co, this corresponds to the oxidation of Co^{3+} to Co^{4+}, whereas for the Mn the shift in the XANES data is attributed to changes in the coordination environment rather than oxidation, with Mn remaining in the 4+ oxidation state.[42] The XANES spectra for the coated and bare electrodes following charging to 4.5 V overlay for both the Co and the Mn; however, when the spectra are considered at a capacity where 50% of the Li^+ ions have been removed, it can be seen that the XANES of the ALD coating is not shifted as high in energy compared to the bare electrode. This shows that the ALD coating is reducing the transformation of the Co and Mn environments by preserving the original layered structure, with charge compensation coming predominantly from the Ni.

Linear combination fitting of the XANES spectra was used to further understand the effect of the ALD coating on the behavior of the transition metal ions. As the bare electrodes showed a greater shift in the XANES spectra at $Li_{0.5}$, the OCV

DOI: 10.1021/acs.chemmater.5b02952
Chem. Mater. 2015, 27, 6146−6154

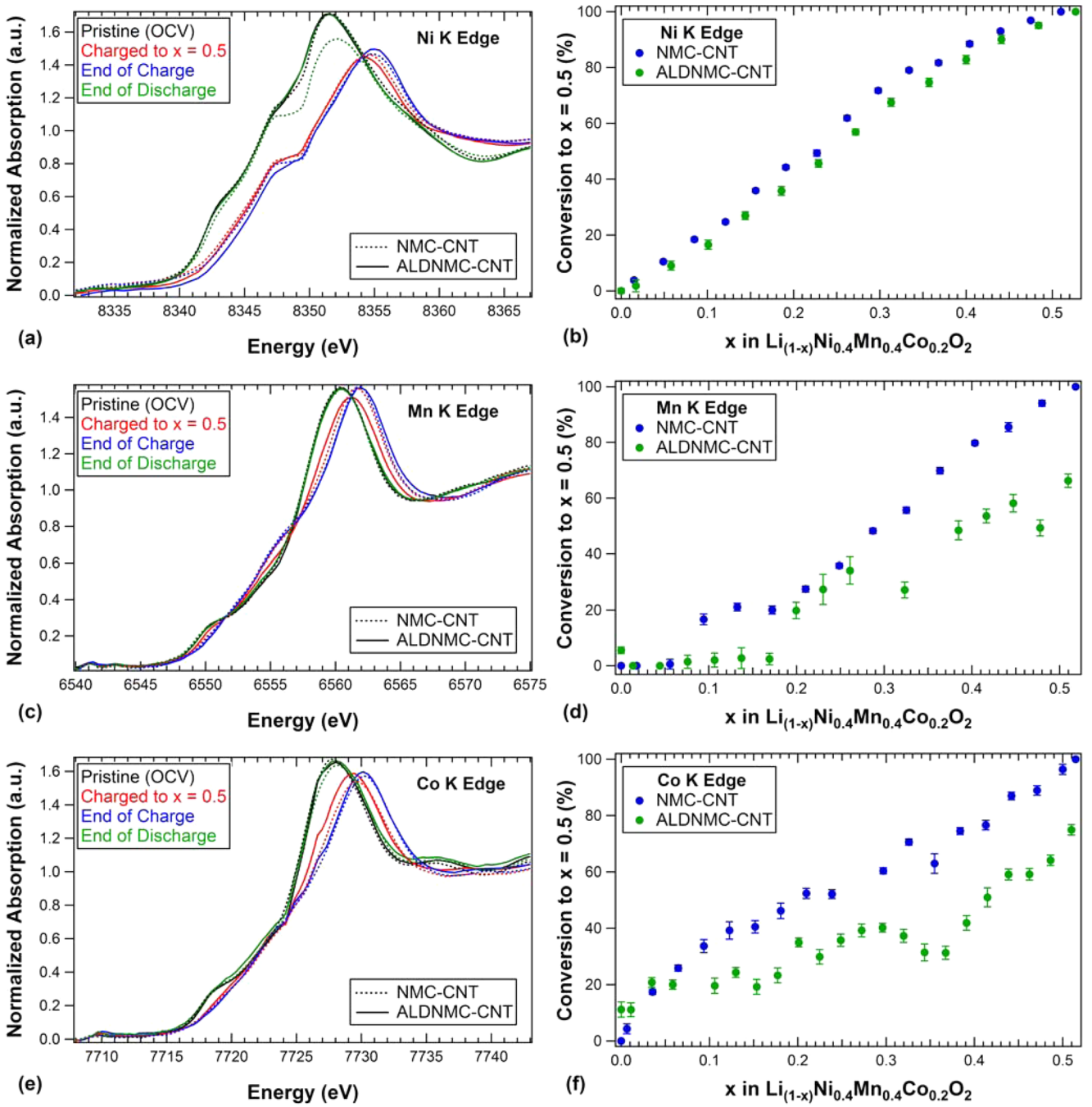

Figure 7. Operando XANES spectra (left) of the bare and ALD-coated samples at different states of charge (where x corresponds to $Li_{(1-x)}Ni_{0.4}Mn_{0.4}Co_{0.2}O_2$), and the % conversion to $x = 0.5$ obtained from LCF (right) using the data collected at each absorption edge for the bare electrodes at OCV and $x = 0.5$ as fitting standards for both bare and coated samples. Data are shown for the Ni (top), Mn (middle), and Co (bottom) K absorption edge measurements. A fresh electrode was used for data collection at each absorption edge.

and $Li_{0.5}$ spectra for the bare data at each absorption edge were used as standards for the LCF of both bare and coated electrodes. The percent conversion of the electrodes from OCV to a capacity where x = 0.5 determined from the LCF is shown in Figure 7b, d, f. The rate of conversion for the Ni electrodes is equivalent for the bare and coated electrodes, with the oxidation of Ni beginning immediately with charging. A significant difference between the NMC−CNT and ALDNMC−CNT is seen in the behavior at the Mn and Co edges, with a clear delay in the onset of Co and Mn transformation in the coated samples. The behavior of the Mn appears to be correlated to the oxidation of Co which might indicate close proximity of the ions as a result of Ni segregation as suggested by the evidence of surface effects in the XANES data recorded at OCV. The delay of the onset of Co oxidation supports the findings from the impedance and XRD data that the ALD coating protects the electrode, in particular, the highly reactive, nucleophilic oxygen associated with the Ni, from side reactions with the electrolyte. This protection of the Ni means that charge compensation can be achieved via the oxidation of Ni at lower potentials, thus reducing the oxidation of Co^{3+} to Co^{4+}, which results in the

DOI: 10.1021/acs.chemmater.5b02952
Chem. Mater. 2015, 27, 6146−6154

release of reactive oxygen. These data show that the preservation of the surface chemistry by the Al_2O_3 coating allows the Li deintercalation to proceed primarily with charge compensation from the oxidation of Ni, enabling reversible cycling behavior.

SUMMARY AND CONCLUSIONS

The combination of electrochemical impedance spectroscopy, operando X-ray diffraction and operando X-ray absorption spectroscopy has been used to investigate the origin of the stability of $LiNi_{0.4}Mn_{0.4}Co_{0.2}O_2$−CNT cathodes at high operating voltages afforded by an ultrathin Al_2O_3 coating. The large increase in impedance seen for the bare NMC−CNT when charged above 4.5 V due to the precipitation of a surface film was mitigated for the ALDNMC−CNT, demonstrating that the Al_2O_3 coating prevents the severe interaction of the surface of the layered oxide with the electrolyte at high voltages. The operando XRD data revealed some irreversibility in the shift in *d*-spacing following charge to 4.7 V, with the coated electrode displaying a higher level of reversibility. The lattice changes associated with lithium deintercalation and intercalation were not restricted by the coating. Additional capacity observed for the bare electrode at higher voltages was attributed to the interaction of the cathode with the electrolyte, in agreement with the EIS data. The role of the coating was further explored at lower voltages by operando XANES measurements. It was observed that the coating suppressed the transformation of Co and Mn at low capacities, which can be attributed to the protection of the Ni by preventing side reactions of the highly reactive oxygen at the Ni sites with the electrolyte and enabling reversible cycling of Ni, the oxidation of which is the major pathway for charge compensation during delithiation.

To conclude, the multimodal approach of in situ EIS, operando XRD, and operando XANES measurements used in this study has enabled the protection of the surface chemistry by the ALD Al_2O_3 coating to be identified as the critical mechanism resulting in the enhanced high rate and high voltage cycling stability of $LiNi_{0.4}Mn_{0.4}Co_{0.2}O_2$−CNT cathodes. This combination of in situ and operando techniques has proven to be a powerful tool which can be applied to further the understanding of other factors influencing the performance of these electrochemical energy storage systems, such as the effect of additives in the electrolyte.

ASSOCIATED CONTENT

Supporting Information

The Supporting Information is available free of charge on the ACS Publications website at DOI: 10.1021/acs.chemmater.5b02952.

High voltage cycling performance with and without HFiP additive, cycling data recorded during operando X-ray measurements, and full diffraction patterns for the coated and bare electrodes (PDF)

AUTHOR INFORMATION

Corresponding Authors

*E-mail: mftoney@slac.stanford.edu.

*E-mail: chunmei.ban@nrel.gov.

Present Addresses

[§]S.M. is currently at New Technologies-Inorganic Materials, BASF, The Netherlands

[#]Z.W. is currently at Institute of Functional Material, College of Science, Donghua University, Shanghai, China 201620.

[||]Z.L. is currently at Department of Materials Science and Engineering, Massachusetts Institute of Technology, Cambridge, MA 02139, USA.

Author Contributions

All authors have given approval to the final version of the manuscript.

Notes

The authors declare no competing financial interest.

ACKNOWLEDGMENTS

This work was supported by the Assistant Secretary for Energy Efficiency and Renewable Energy, Office of Vehicle Technologies, for the U.S. Department of Energy under Contract DE-AC-36-08GO28308, subcontract NFT-8-88527-01 under the Batteries for Advanced Transportation Technologies Program (now Advanced Battery Materials Research), and by the Department of Energy, Laboratory Directed Research and Development funding at SLAC National Accelerator Laboratory under Contract DE-AC02-76SF00515. Use of the Stanford Synchrotron Radiation Lightsource, SLAC National Accelerator Laboratory, is supported by the U.S. Department of Energy, Office of Science, Office of Basic Energy Sciences, under Contract DE-AC02-76SF00515.

REFERENCES

(1) Whittingham, M. S. Ultimate Limits to Intercalation Reactions for Lithium Batteries. *Chem. Rev.* **2014**, *114*, 11414−11443.

(2) Tarascon, J. M.; Armand, M. Issues and Challenges Facing Rechargeable Lithium Batteries. *Nature* **2001**, *414*, 359−367.

(3) Aurbach, D. Review of Selected Electrode-Solution Interactions which Determine the Performance of Li and Li-ion Batteries. *J. Power Sources* **2000**, *89*, 206−218.

(4) Goodenough, J. B.; Kim, Y. Challenges for Rechargeable Li Batteries. *Chem. Mater.* **2010**, *22*, 587−603.

(5) Xu, K. Electrolytes and Interphases in Li-ion Batteries and Beyond. *Chem. Rev.* **2014**, *114*, 11503−618.

(6) Li, C.; Zhang, H. P.; Fu, L. J.; Liu, H.; Wu, Y. P.; Rahm, E.; Holze, R.; Wu, H. Q. Cathode Materials Modified by Surface Coating for Lithium Ion Batteries. *Electrochim. Acta* **2006**, *51*, 3872−3883.

(7) Fu, L. J.; Liu, H.; Li, C.; Wu, Y. P.; Rahm, E.; Holze, R.; Wu, H. Q. Surface Modifications of Electrode Materials for Lithium Ion Batteries. *Solid State Sci.* **2006**, *8*, 113−128.

(8) Groner, M. D.; Fabreguette, F. H.; Elam, J. W.; George, S. M. Low-temperature Al_2O_3 Atomic Layer Deposition. *Chem. Mater.* **2004**, *16*, 639−645.

(9) Jung, Y. S.; Cavanagh, A. S.; Dillon, A. C.; Groner, M. D.; George, S. M.; Lee, S. H. Enhanced Stability of $LiCoO_2$ Cathodes in Lithium-ion Batteries Using Surface Modification by Atomic Layer Deposition. *J. Electrochem. Soc.* **2010**, *157*, A75−A81.

(10) Jung, Y. S.; Lu, P.; Cavanagh, A. S.; Ban, C.; Kim, G. H.; Lee, S. H.; George, S. M.; Harris, S. J.; Dillon, A. C. Unexpected Improved Performance of ALD Coated $LiCoO_2$/graphite Li-ion Batteries. *Adv. Energy Mater.* **2013**, *3*, 213−219.

(11) Yabuuchi, N.; Ohzuku, T. Novel Lithium Insertion Material of $LiCo_{1/3}Ni_{1/3}Mn_{1/3}O_2$ for Advanced Lithium-ion Batteries. *J. Power Sources* **2003**, *119*, 171−174.

(12) Yabuuchi, N.; Makimura, Y.; Ohzuku, T. Solid-state Chemistry and Electrochemistry of $LiCo_{1/3}Ni_{1/3}Mn_{1/3}O_2$ for Advanced Lithium-ion Batteries III. Rechargeable Capacity and Cycleability. *J. Electrochem. Soc.* **2007**, *154*, A314−A321.

(13) Ngala, J. K.; Chernova, N. A.; Ma, M. M.; Mamak, M.; Zavalij, P. Y.; Whittingham, M. S. The Synthesis, Characterization and Electrochemical Behavior of the Layered $LiNi_{0.4}Mn_{0.4}Co_{0.2}O_2$ Compound. *J. Mater. Chem.* **2004**, *14*, 214−220.

DOI: 10.1021/acs.chemmater.5b02952
Chem. Mater. 2015, 27, 6146−6154

(14) Ma, M. M.; Chernova, N. A.; Toby, B. H.; Zavalij, P. Y.; Whittingham, M. S. Structural and Electrochemical Behavior of $LiMn_{0.4}Ni_{0.4}Co_{0.2}O_2$. *J. Power Sources* **2007**, *165*, 517−534.
(15) Li, Z.; Ban, C.; Chernova, N. A.; Wu, Z.; Upreti, S.; Dillon, A.; Whittingham, M. S. Towards Understanding the Rate Capability of Layered Transition Metal Oxides $LiNi_yMn_yCo_{1-2y}O_2$. *J. Power Sources* **2014**, *268*, 106−112.
(16) Li, Z.; Chernova, N. A.; Roppolo, M.; Upreti, S.; Petersburg, C.; Alamgir, F. M.; Whittingham, M. S. Comparative Study of the Capacity and Rate Capability of $LiNi_yMn_yCo_{1-2y}O_2$ (y = 0.5, 0.45, 0.4, 0.33). *J. Electrochem. Soc.* **2011**, *158*, A516−A522.
(17) Cho, Y. H.; Jang, D.; Yoon, J.; Kim, H.; Ahn, T. K.; Nam, K. W.; Sung, Y. E.; Kim, W. S.; Lee, Y. S.; Yang, X. Q.; Yoon, W. S. Thermal Stability of Charged $LiNi_{0.5}Co_{0.2}Mn_{0.3}O_2$ Cathode for Li-ion Batteries Investigated by Synchrotron Based in situ X-ray Diffraction. *J. Alloys Compd.* **2013**, *562*, 219−223.
(18) Hwang, B. J.; Hu, S. K.; Chen, C. H.; Chen, C. Y.; Sheu, H. S. In-situ XRD Investigations on Structure Changes of ZrO_2-coated $LiMn_{0.5}Ni_{0.5}O_2$ Cathode Materials During Charge. *J. Power Sources* **2007**, *174*, 761−765.
(19) Kim, J. W.; Travis, J. J.; Hu, E. Y.; Nam, K. W.; Kim, S. C.; Kang, C. S.; Woo, J. H.; Yang, X. Q.; George, S. M.; Oh, K. H.; Cho, S. J.; Lee, S. H. Unexpected High Power Performance of Atomic Layer Deposition Coated $Li[Ni_{1/3}Mn_{1/3}Co_{1/3}]O_2$ Cathodes. *J. Power Sources* **2014**, *254*, 190−197.
(20) Zhang, X. F.; Belharouak, I.; Li, L.; Lei, Y.; Elam, J. W.; Nie, A. M.; Chen, X. Q.; Yassar, R. S.; Axelbaum, R. L. Structural and Electrochemical Study of Al_2O_3 and TiO_2 Coated $Li_{1.2}Ni_{0.13}Mn_{0.54}Co_{0.13}O_2$ Cathode Material Using ALD. *Adv. Energy Mater.* **2013**, *3*, 1299−1307.
(21) Bhuvaneswari, D.; Babu, G.; Kalaiselvi, N. Effect of Surface Modifiers in Improving the Electrochemical Behavior of $LiNi_{0.4}Mn_{0.4}Co_{0.2}O_2$ Cathode. *Electrochim. Acta* **2013**, *109*, 684−693.
(22) Meng, X. B.; Yang, X. Q.; Sun, X. L. Emerging Applications of Atomic Layer Deposition for Lithium-ion Battery Studies. *Adv. Mater.* **2012**, *24*, 3589−3615.
(23) Chung, K. Y.; Yoon, W. S.; Lee, H. S.; McBreen, J.; Yang, X. Q.; Oh, S. H.; Ryu, W. H.; Lee, J. L.; Won, I. C.; Cho, B. W. In situ XRD Studies of the Structural Changes of ZrO_2-coated $LiCoO_2$ During Cycling and Their Effects on Capacity Retention in Lithium Batteries. *J. Power Sources* **2006**, *163*, 185−190.
(24) Chung, K. Y.; Yoon, W. S.; McBreen, J.; Yang, X. Q.; Oh, S. H.; Shin, H. C.; Cho, W. I.; Cho, B. W. In situ X-ray Diffraction Studies on the Mechanism of Capacity Retention Improvement by Coating at the Surface of $LiCoO_2$. *J. Power Sources* **2007**, *174*, 619−623.
(25) Liu, L. J.; Chen, L. Q.; Huang, X. J.; Yang, X. Q.; Yoon, W. S.; Lee, H. S.; McBreen, J. Electrochemical and in situ Synchrotron XRD Studies on Al_2O_3-coated $LiCoO_2$ Cathode Material. *J. Electrochem. Soc.* **2004**, *151*, A1344−A1351.
(26) Taguchi, N.; Akita, T.; Sakaebe, H.; Tatsumi, K.; Ogumi, Z. Characterization of the Surface of $LiCoO_2$ Particles Modified by Al and Si Oxide Using Analytical TEM. *J. Electrochem. Soc.* **2013**, *160*, A2293−A2298.
(27) Verdier, S.; El Ouatani, L.; Dedryvere, R.; Bonhomme, F.; Biensan, P.; Gonbeau, D. XPS Study on Al_2O_3- and $AlPO_4$-coated $LiCoO_2$ Cathode Material for High-capacity Li-ion Batteries. *J. Electrochem. Soc.* **2007**, *154*, A1088−A1099.
(28) Lu, Y. C.; Mansour, A. N.; Yabuuchi, N.; Shao-Horn, Y. Probing the Origin of Enhanced Stability of "$AlPO_4$" Nanoparticle Coated $LiCoO_2$ During Cycling to High Voltages: Combined XRD and XPS studies. *Chem. Mater.* **2009**, *21*, 4408−4424.
(29) Zeng, D. L.; Cabana, J.; Breger, J. L.; Yoon, W. S.; Grey, C. P. Cation Ordering in $Li[NixMnxCo_{1-2x}]O_2$-layered Cathode Materials: A Nuclear Magnetic Resonance (NMR), Pair Distribution Function, X-ray Absorption Spectroscopy, and Electrochemical Study. *Chem. Mater.* **2007**, *19*, 6277−6289.
(30) Zeng, D.; Cabana, J.; Yoon, W.-S.; Grey, C. P. Investigation of the Structural Changes in $Li[Ni_yMn_yCo_{1-2y}]O_2$(y= 0.05) upon Electrochemical Lithium Deintercalation. *Chem. Mater.* **2010**, *22*, 1209−1219.
(31) Ban, C. M.; Li, Z.; Wu, Z. C.; Kirkham, M. J.; Chen, L.; Jung, Y. S.; Payzant, E. A.; Yan, Y. F.; Whittingham, M. S.; Dillon, A. C. Extremely Durable High-rate Capability of a $LiNi_{0.4}Mn_{0.4}Co_{0.2}O_2$ Cathode Enabled with Single-walled Carbon Nanotubes. *Adv. Energy Mater.* **2011**, *1*, 58−62.
(32) Dillon, A. C.; Gennett, T.; Jones, K. M.; Alleman, J. L.; Parilla, P. A.; Heben, M. J. A Simple and Complete Purification of Single-walled Carbon Nanotube Materials. *Adv. Mater.* **1999**, *11*, 1354−1358.
(33) Lande, J.; Webb, S.; Mehta, A. *Area Diffraction Machine*; https://github.com/joshualande/AreaDiffractionMachine.
(34) Ravel, B.; Newville, M. ATHENA, ARTEMIS, HEPHAESTUS: Data Analysis for X-ray Absorption Spectroscopy Using IFEFFIT. *J. Synchrotron Radiat.* **2005**, *12*, 537−541.
(35) Hwang, B. J.; Tsai, Y. W.; Carlier, D.; Ceder, G. A Combined Computational/Experimental Study on $LiNi_{1/3}Co_{1/3}Mn_{1/3}O_2$. *Chem. Mater.* **2003**, *15*, 3676−3682.
(36) Atebamba, J. M.; Moskon, J.; Pejovnik, S.; Gaberscek, M. On the Interpretation of Measured Impedance Spectra of Insertion Cathodes for Lithium-ion Batteries. *J. Electrochem. Soc.* **2010**, *157*, A1218−A1228.
(37) Martha, S. K.; Sclar, H.; Framowitz, Z. S.; Kovacheva, D.; Saliyski, N.; Gofer, Y.; Sharon, P.; Golik, E.; Markovsky, B.; Aurbach, D. A Comparative Study of Electrodes Comprising Nanometric and Submicron Particles of $LiNi_{0.5}0Mn_{0.50}O_2$, $LiNi_{0.33}Mn0.33Co_{0.33}O_2$, and $LiNi_{0.40}Mn_{0.40}Co_{0.20}O_2$ Layered Compounds. *J. Power Sources* **2009**, *189*, 248−255.
(38) Yang, X. Q.; Sun, X.; McBreen, J. New Findings on the Phase Transitions in $Li_{1-x}NiO_2$: in situ Synchrotron X-ray Diffraction Studies. *Electrochem. Commun.* **1999**, *1*, 227−232.
(39) Yoon, W. S.; Chung, K. Y.; McBreen, J.; Yang, X. Q. A Comparative Study on Structural Changes of $LiCo_{1/3}Ni_{1/3}Mn_{1/3}O_2$ and $LiNi_{0.8}Co_{0.15}Al_{0.05}O_2$ During First Charge Using in situ XRD. *Electrochem. Commun.* **2006**, *8*, 1257−1262.
(40) Breger, J.; Meng, Y. S.; Hinuma, Y.; Kumar, S.; Kang, K.; Shao-Horn, Y.; Ceder, G.; Grey, C. P. Effect of High Voltage on the Structure and Electrochemistry of $LiNi_{0.5}Mn_{0.5}O_2$: A Joint Experimental and Theoretical Study. *Chem. Mater.* **2006**, *18*, 4768−4781.
(41) Rumble, C.; Conry, T. E.; Doeff, M.; Cairns, E. J.; Penner-Hahn, J. E.; Deb, A. Structural and Electrochemical Investigation of Li $(Ni_{0.4}Co_{0.15}Al_{0.05}Mn_{0.4})O_2$ Cathode Material. *J. Electrochem. Soc.* **2010**, *157*, A1317−A1322.
(42) Deb, A.; Bergmann, U.; Cramer, S. P.; Cairns, E. J. In situ X-ray Absorption Spectroscopic Study of the $Li[Ni_{1/3}Co_{1/3}Mn_{1/3}]O_2$ Cathode Material. *J. Appl. Phys.* **2005**, *97*, 113523.
(43) Gu, M.; Genc, A.; Belharouak, I.; Wang, D.; Amine, K.; Thevuthasan, S.; Baer, D. R.; Zhang, J.-G.; Browning, N. D.; Liu, J.; Wang, C. Nanoscale Phase Separation, Cation Ordering, and Surface Chemistry in Pristine $Li_{1.2}Ni_{0.2}Mn_{0.6}O_2$for Li-ion Batteries. *Chem. Mater.* **2013**, *25*, 2319−2326.

DOI: 10.1021/acs.chemmater.5b02952
Chem. Mater. 2015, 27, 6146−6154